5. Y. Wu, N. Murray, *Astrophys. J.* **589**, 605–614 (2003).
6. S. Naoz, W. M. Farr, Y. Lithwick, F. A. Rasio, J. Teyssandier, *Nature* **473**, 187–189 (2011).
7. G. Takeda, F. A. Rasio, *Astrophys. J.* **627**, 1001–1010 (2005).
8. M. Jurić, S. Tremaine, *Astrophys. J.* **686**, 603–620 (2008).
9. D. Fabrycky, S. Tremaine, *Astrophys. J.* **669**, 1298–1315 (2007).
10. Y. Wu, N. W. Murray, J. M. Ramsahai, *Astrophys. J.* **670**, 820–825 (2007).
11. S. Chatterjee, E. B. Ford, S. Matsumura, F. A. Rasio, *Astrophys. J.* **686**, 580–602 (2008).
12. M. Nagasawa, S. Ida, *Astrophys. J.* **742**, 72 (2011).
13. T. D. Morton, J. A. Johnson, *Astrophys. J.* **738**, 170 (2011).
14. S. Naoz, W. M. Farr, F. A. Rasio, *Astrophys. J. Lett.* **754**, L36 (2012).
15. E. J. Rivera *et al.*, *Astrophys. J.* **719**, 890–899 (2010).
16. R. Sanchis-Ojeda *et al.*, *Nature* **487**, 449–453 (2012).
17. M. H. Lee, S. J. Peale, *Astrophys. J.* **567**, 596–609 (2002).
18. B. E. McArthur *et al.*, *Astrophys. J.* **715**, 1203–1220 (2010).
19. R. I. Dawson *et al.*, *Astrophys. J.* **71**, 89 (2014).
20. A. Cumming *et al.*, *Publ. Astron. Soc. Pac.* **120**, 531–554 (2008).
21. C. Petrovich, S. Tremaine, R. Rafikov, *Astrophys. J.* **786**, 101 (2014).
22. A. Socrates, B. Katz, S. Dong, http://arxiv.org/abs/1209.5724 (2012).
23. S. Dong, B. Katz, A. Socrates, *Astrophys. J. Lett.* **781**, L5 (2014).
24. C. Petrovich, http://arxiv.org/abs/1405.0280 (2014).
25. H. A. Knutson *et al.*, *Astrophys. J.* **785**, 126 (2014).
26. R. I. Dawson, R. A. Murray-Clay, *Astrophys. J. Lett.* **767**, L24 (2013).
27. E. I. Chiang, S. Tabachnik, S. Tremaine, *Astron. J.* **122**, 1607–1615 (2001).
28. T. A. Michtchenko, R. Malhotra, *Icarus* **168**, 237–248 (2004).
29. Queried from the Exoplanet Orbit Database (EOD) at exoplanets.org (*50*) on 8 April 2014.
30. Eccentricity was detected at two-sigma, and $\Delta\omega_{sky}$ was detected with an uncertainty of <40°.
31. We selected for eccentric warm Jupiters with only one known companion, because additional companions can disrupt Kozai oscillations. Our selection criterion thus excludes planetary pairs that are members of the 55 Cnc, upsilon Andromeda, mu Arae, HIP 14810, Kepler-9, and Kepler-30 systems. Moreover, each of these systems also has a close-in (a < 0.1 AU) planet that would be disrupted if the warm Jupiter were to attain periapse distances small enough for tidal circularization.
32. X. Tan *et al.*, *Astrophys. J.* **777**, 101 (2013).
33. For HD 202206c, modification of the semimajor axis from the best-fit value was required to avoid libration in the 5:1 resonance. See the supplementary materials for details.
34. J. E. Chambers, *Mon. Not. R. Astron. Soc.* **304**, 793–799 (1999).
35. D. C. Fabrycky, in *Exoplanets*, S. Seager, Ed. (Univ. of Arizona Press, Tuscon, AZ, 2011), pp. 217–238.
36. D. Veras, E. B. Ford, *Astrophys. J.* **715**, 803–822 (2010).
37. A. L. Whipple, P. J. Shelus, *Icarus* **101**, 265–271 (1993).
38. J. Correa Otto, A. M. Leiva, C. A. Giuppone, C. Beaugé, *Mon. Not. R. Astron. Soc.* **402**, 1959–1968 (2010).
39. T. Yokoyama, M. T. Santos, G. Cardin, O. C. Winter, *Astron. Astrophys.* **401**, 763–772 (2003).
40. E. B. Ford, B. Kozinsky, F. A. Rasio, *Astrophys. J.* **535**, 385–401 (2000).
41. R. Barnes, R. Greenberg, *Astrophys. J. Lett.* **659**, L53–L56 (2007).
42. E. B. Ford, *IAU Symp.* **249**, 441–446 (2008).
43. B. Katz, S. Dong, R. Malhotra, *Phys. Rev. Lett.* **107**, 181101 (2011).
44. Y. Lithwick, S. Naoz, *Astrophys. J.* **742**, 94 (2011).
45. S. Naoz, W. M. Farr, Y. Lithwick, F. A. Rasio, J. Teyssandier, *Mon. Not. R. Astron. Soc.* **431**, 2155–2171 (2013).
46. G. Li, S. Naoz, B. Kocsis, A. Loeb, *Astrophys. J.* **785**, 116 (2014).
47. G. Li, S. Naoz, M. Holman, A. Loeb, *Astrophys. J.* **791**, 86 (2014).
48. L. G. Kiseleva, P. P. Eggleton, S. Mikkola, *Mon. Not. R. Astron. Soc.* **300**, 292–302 (1998).
49. The eccentricity of HD 202206b does not have such an envelope (fig. S5), which may be due to its proximity to the 5:1 mean-motion resonance and the large relative mass of the inner planet.
50. J. T. Wright *et al.*, *Publ. Astron. Soc. Pac.* **123**, 412–422 (2011).
51. Among the black diamonds, the planetary pairs with $|\Delta\omega_{sky}|$ near 90° and large angular momentum ratios include giant planets in a five-planet system (55 Cnc), a pair of hot super-Earths (GJ 163), and a cold Jupiter partnered with a hot Neptune (HD 125612); it is unclear whether their orthogonal eccentricity vectors also signify large mutual inclinations. The transiting pair Kepler-30 c and d, which are near a 2:1 resonance, have $|\Delta\omega_{sky}|$ = 114°, an angular momentum ratio of 21, and a low mutual inclination (*16*).

ACKNOWLEDGMENTS

We gratefully acknowledge support from the Miller Institute for Basic Research in Science, the University of California (UC) Berkeley's Center for Integrative Planetary Science, the National Science Foundation, and the National Aeronautics and Space Administration. This research has made use of the Exoplanet Orbit Database at exoplanets.org. This research employed the SAVIO computational cluster provided by the Berkeley Research Computing program, which is supported by UC Berkeley's Chancellor, Vice Chancellor for Research, and Chief Information Officer. We thank four anonymous referees for constructive feedback and D. Fabrycky and J. Johnson for helpful comments.

SUPPLEMENTARY MATERIALS

www.sciencemag.org/content/346/6206/212/suppl/DC1
Figs. S1 to S7
Table S1
References (*52*–*63*)

4 June 2014; accepted 12 September 2014
10.1126/science.1256943

EARLY UNIVERSE

A local clue to the reionization of the universe

Sanchayeeta Borthakur,[1]* Timothy M. Heckman,[1] Claus Leitherer,[2] Roderik A. Overzier[3]

Identifying the population of galaxies that was responsible for the reionization of the universe is a long-standing quest in astronomy. We present a possible local analog that has an escape fraction of ionizing flux of 21%. Our detection confirms the existence of gaps in the neutral gas enveloping the starburst region. The candidate contains a massive yet highly compact star-forming region. The gaps are most likely created by the unusually strong winds and intense ionizing radiation produced by this extreme object. Our study also validates the indirect technique of using the residual flux in saturated low-ionization interstellar absorption lines for identifying such leaky galaxies. Because direct detection of ionizing flux is impossible at the epoch of reionization, this represents a highly valuable technique for future studies.

The reionization of the universe is a crucial event in cosmic history. Identifying the source(s) responsible for reionization will allow us to understand the underlying physics. Star-forming galaxies are the most likely candidates, but what is their nature? By what process does Lyman continuum radiation, capable of ionizing hydrogen atoms, escape the region of dense and cold gas from which the required population of hot massive stars forms?

Studies to date have had limited success at detecting such candidates. For example, Iwata *et al.* (*1*) found continuum leaking out of 17 galaxies from their sample of 198 star-forming galaxies [Lyman break galaxies (LBGs) and Lyα emitters (LAEs)], whereas Vanzella *et al.* (*2*) found only one such leaking galaxy out of 102 LBGs. Most of the high-redshift studies have resulted in only a handful of detections with substantial escape fractions (*3*, *4*). In some ways, the low incidence of such galaxies is not surprising. Hot massive stars are located in gas-rich regions with column densities ranging from 10^{21} to 10^{24} cm^{-2}. This is 4 to 7 orders of magnitude higher than the column density of H I required to produce an optical depth of unity at the Lyman edge ($N = 1.4 \times 10^{17}$ cm^{-2}). Therefore, extreme conditions may be required for a substantial fraction of the ionizing flux to escape from the galaxy.

Identifying local examples of such leaky galaxies will allow us to study in detail the processes that lead to the escape of Lyman continuum radiation. These local examples can also be used to validate indirect signatures of escaping ionizing flux that are based on the properties of the spectrum at wavelengths longer than the Lyman-α line (see below). This is invaluable, because the spectral region at shorter wavelengths is completely opaque at the epoch of recombination.

We previously uncovered a sample of relatively rare local (redshift $z \approx 0.2$) starburst galaxies whose overall properties [mass, metallicity, size, morphology, star formation rate, kinematics, dust attenuation, etc.] are very similar to those of the LBGs (*5*–*10*). These galaxies are termed Lyman break analog galaxies (LBAs). SDSS J092159.38+450912.3 (hereafter J0921+4509) is one such local LBA (z = 0.23499) that is producing stars at the rate of 50 solar masses ($M_\odot$) per year. It belongs to a special class of LBA where several billion solar masses of stars are produced in an extremely compact central region with a radius of ~100 pc (*11*). Such massive and highly

[1]Center for Astrophysical Sciences, Department of Physics and Astronomy, Johns Hopkins University, Baltimore, MD 21218, USA. [2]Space Telescope Science Institute, 3700 San Martin Drive, Baltimore, MD 21218, USA. [3]Observatório Nacional, Ministry of Science, Technology, and Innovation, Rio de Janeiro, Brazil.
*Corresponding author. E-mail: sanch@pha.jhu.edu

here, which produces warm Jupiters with the observed clustering of $|\Delta\omega_{sky}|$ near 90°, is complementary: Both the inner and outer planets' eccentricities are too modest for the octupolar potential to effect flips, and i_{mut} remains near 40°, a prograde configuration. We deduced that our six systems with warm Jupiters and close friends are prograde, with $i_{mut} \sim 40°$ rather than retrograde with $i_{mut} \sim 140°$, because in the latter case $\omega_{sky,1} + \omega_{sky,2}$ would librate rather than $\omega_{sky,1} - \omega_{sky,2}$ (*39*).

It is no coincidence that our six warm Jupiter systems are all characterized by mutual inclinations abutting Kozai's minimum angle. In our regime in which the quadrupole potential still dominates and planetary eccentricities are low enough to avoid flips, 39° is the inclination that coincides with maximum eccentricity (minimum periapse) and hence maximum tidal dissipation. Orbital decay during this maximum-eccentricity, minimum-inclination phase of the Kozai cycle naturally leads to an abundance of tidally migrated warm Jupiters with i_{mut} near 39° to 65° (*48*). The octupolar potential is not strong enough for our systems to alter this feature of quadrupolar Kozai cycles (*6*, *48*). At the same time, the reason why warm Jupiters have not completed their migration to become hot Jupiters is because of the special octupole-modified nature of their eccentricity variations. The usual (quadrupole) Kozai oscillations of eccentricity, which occur over the short nodal precession period, are modulated by an octupole-induced envelope (*49*) of much longer period following that of apsidal libration (Fig. 3 and figs. S1 to S5). The envelope period is approximately $(a_2/a_1)(1 - e_2^2)/e_2$ longer than the Kozai time scale (*46*). This long-period modulation prevents eccentricities from surging too often and renders migration even slower than the "slow Kozai" migration described in (*24*). Such "super slow" evolution is similar to the "step" migration seen at high i_{mut} (*6*), except without the transition from prograde to retrograde orbital motion and the accompanying rapid tidal circularization. In the gentle and intermittent migration considered here, warm Jupiters reach the small periapses characterizing hot Jupiters only at the peaks of their eccentricity envelopes. As a proof of concept, we performed an integration of the secular equations of motion including tidal friction (Fig. 4). The warm Jupiter undergoes super slow tidal migration in which it librates apsidally and stalls in semimajor axis. A libration amplitude for $\Delta\varpi_{inv}$ near 90° enables super slow migration. If the libration amplitude were smaller, or if the apsidal separation were to circulate, then the envelope modulating the eccentricity would be less peaky, and the interior planet would spend more of its time near its maximum eccentricity. If the libration amplitude were larger, then not only would the apsidal separation be more prone to circulate given a small perturbation, but the system would also be more vulnerable to retrograde flips and concomitant eccentricity surges ($e \rightarrow 1$). The upshot of all these scenarios (fig. S7) in which $\Delta\varpi_{inv}$ does not librate with an amplitude of 90° is that tidal migration, once begun, would rapidly complete and spawn a hot Jupiter.

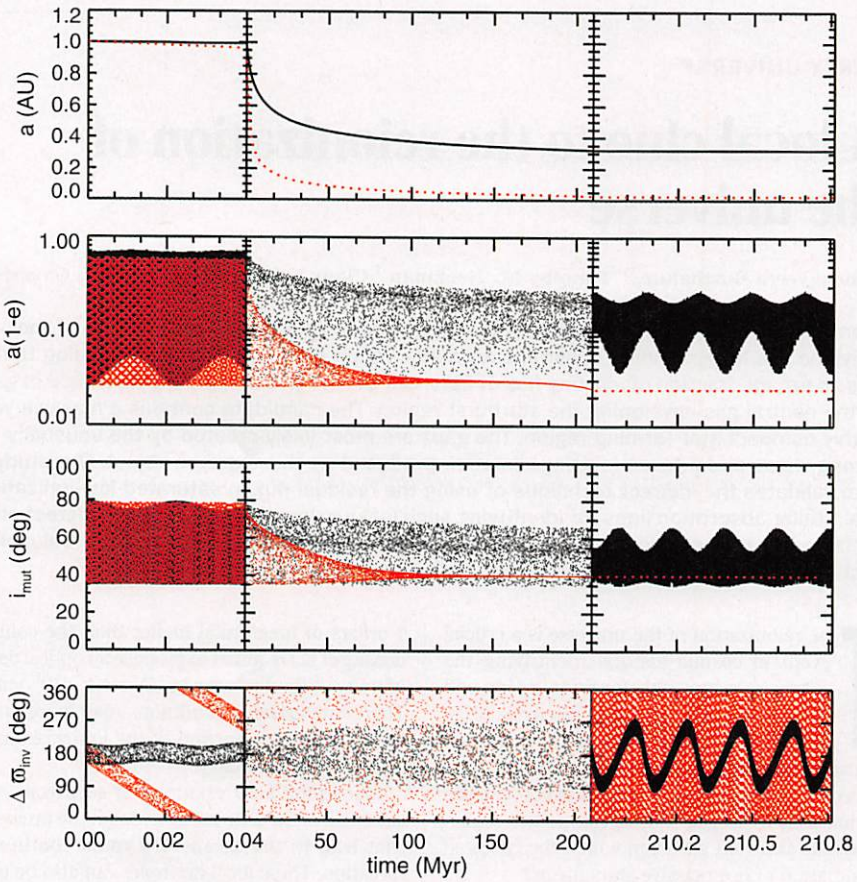

Fig. 4. Tidal migration under a secular potential expanded beyond quadrupolar order can produce a stalled warm Jupiter. Plotted are the time evolution of the inner planet's semimajor axis, periapse distance, mutual inclination with the outer planet, and apsidal separation, integrated using the test particle Hamiltonian expanded to hexadecapolar order (*39*); practically identical results are obtained with the octupolar Hamiltonian. Overplotted are results from the Hamiltonian including only up to quadrupolar terms (red dashed line) in which the inner planet fails to stall and instead becomes a hot Jupiter. General-relativistic precession is included for both planets (*35*). Tidal evolution was implemented using a constant tidal quality factor of 10^5, a Love number of 0.26, and a planetary radius of 1 Jupiter radius (*5*). Tides raised on the star are not included because they are weak compared to tides raised on the planet at these semimajor axes. The tidal forcing frequency is set to $\sqrt{\frac{G(M_* + m_1)}{|a_1(1 - e_1^2)|^3}}$ (*22*). The outer planet has $a_2 = 1.923$ AU, $e_2 = 0.133$, and $m_2 = 6.59\ M_{Jupiter}$, matching HD 147018c, and initial $\{i_2 = 0°, \omega_2 = 17.2°, \Omega_2 = 180°\}$. The inner planet (test particle) has initial $a_1 = 1$ AU, $e_1 = 0.9$, and $\{i_1 = 65°, \omega_1 = 38.4°, \Omega_1 = 0°\}$. With these choices, the eccentricity of the inner planet reaches a minimum of 0.33 at time = 220 years during the first Kozai cycle. The early tidal evolution, over the first ~20 million years, is subject to planet-planet scattering in a full *N*-body treatment; as such, the origin story portrayed in this figure is meant only to illustrate the concept of stalling, not to be definitive. This figure ends at ~200 million years, but similar histories spanning a few billion years are just as possible for different initial conditions or tidal efficiency factors.

The class of warm Jupiters we have identified is similar to the predicted class of Kozai-oscillating warm Jupiters (*23*), except that here the octupolar field generated by the eccentricity of the exterior perturber plays a starring role in effecting the observed near-orthogonality of periapse directions and in braking tidal migration. The mutual inclination of $i_{mut} \sim 35°$ to 65° that we have inferred from the measured apsidal misalignment attests to how the Kozai mechanism, working between planets, has indeed shaped planetary systems. Although large inclinations between hot Jupiters' orbital planes and the equatorial planes of their host stars are well established, our finding provides evidence that pairs of more-distant giant planets are themselves highly mutually inclined (although still prograde), in stark contrast to the flatness of solar system planets. The origin of such large inclinations is a mystery; planet-planet scattering (*1*) or secular chaos (*2*) are possibilities.

REFERENCES AND NOTES

1. F. A. Rasio, E. B. Ford, *Science* **274**, 954–956 (1996).
2. Y. Wu, Y. Lithwick, *Astrophys. J.* **735**, 109 (2011).
3. Y. Kozai, *Astron. J.* **67**, 591 (1962).
4. M. L. Lidov, *Planet. Space Sci.* **9**, 719–759 (1962).

compact star-forming regions are referred to as dominant central objects (DCOs). Because of their compact nature, DCOs can generate extreme winds that were found to propel the surrounding interstellar neutral and ionized gas outward at velocities in excess of 1000 km s^{-1} (*9*).

Three independent but indirect lines of evidence were put forth by Heckman *et al.* (*9*) suggesting that a substantial amount of ionizing radiation could be escaping from this galaxy and others with DCOs. First, these authors found that the strongest interstellar absorption lines tracing the neutral phase of the interstellar medium (ISM) were optically thick (saturated) but still had a substantial residual flux in the line cores [~20 to 30%; see (*9*), figures 4 and 5]. This is an indication that the far-ultraviolet (UV) continuum source, the DCO, is only partially covered by optically thick neutral material. Second, they detected a substantial amount of blue-shifted Lyman-α emission, despite the presence of neutral gas seen in absorption at those velocities. This requires only partial coverage of the starburst region by the outflowing neutral gas. Third, the star formation rate estimated for this galaxy based on the extinction-corrected Hα emission line was smaller by a factor of 3 than the value based on the sum of the far-IR and far-UV continuum luminosities. This could indicate that some of the ionizing flux escapes the galaxy and thus does not produce Hα emission by photoionization and recombination. These properties led Heckman *et al.* (*9*) to speculate that the extreme feedback provided by an extraordinarily compact massive starburst (like a DCO) might be required to enable the escape of ionizing radiation from galaxies.

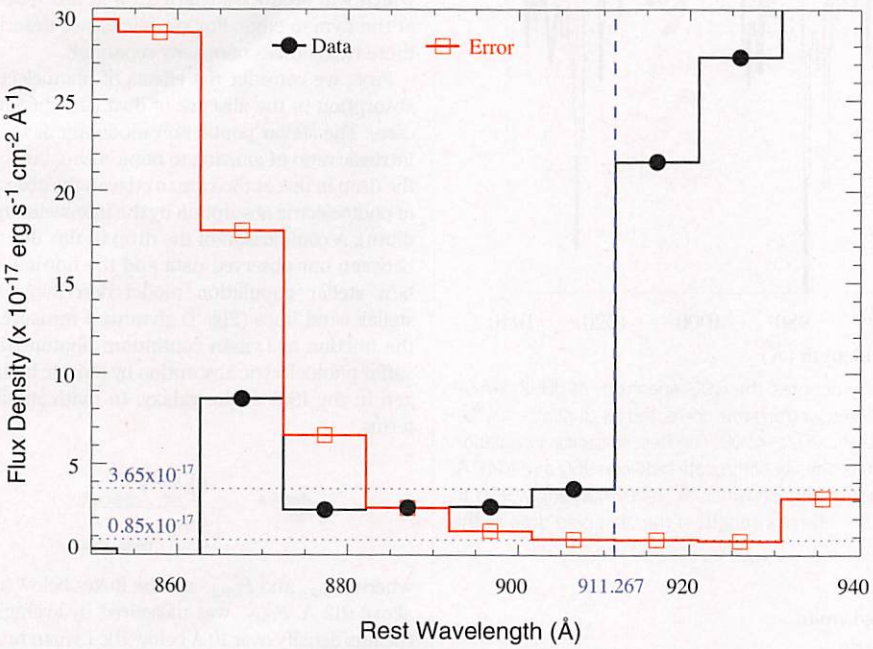

Fig. 1. COS spectra of J0921+4509. Flux density around the rest-frame wavelength 912 Å is shown in black (solid circles) and the associated errors in red (open squares). The flux density and errors were obtained by binning the COS pipeline data by 150 pixels (~10 Å) to increase the signal-to-noise ratio. The dashed blue line marks the position of the Lyman continuum break (≡ 13.6 eV). We detected Lyman continuum flux in the wavelength range 890 to 910 Å. The flux at 910 Å was measured to be 3.7 (±0.8) × 10^{-17} erg s^{-1} cm^{-2} $Å^{-1}$.

To directly confirm the inference of escaping ionizing radiation and compare it to that predicted by the residual flux technique, we conducted a program with the Cosmic Origins Spectrograph (COS) aboard the Hubble Space Telescope (HST) to obtain the spectrum of J0921+4509 below the Lyman edge at 912 Å in the rest frame of the galaxy. The data were obtained in two separate sets of observations (durations 4 and 5 orbits of HST, respectively), which were reduced using the standard COS data reduction pipeline (*12*). The final spectrum (Fig. 1) was produced by binning 150 pixels of the weighted average of the two data sets in order to improve the signal-to-noise ratio. The spectrum was corrected for the Milky Way's dust extinction in the direction of J0921+4509. We report a flux density detection of 3.7 (±0.8) × 10^{-17} erg s^{-1} cm^{-2} $Å^{-1}$ just below the Lyman edge. This corresponds to a luminosity λL_λ, at rest wavelength λ = 910 Å, of 5.0 × 10^{42} erg s^{-1}.

The young stars that produce the ionizing flux also produce strong stellar winds, which can be traced using transitions such as N V and C IV. These transitions are minimally contaminated by interstellar features and have the greatest diagnostic power to identify the underlying stellar populations. The strong P-Cygni profiles in these transitions (Fig. 2) clearly indicate the presence of young massive O stars capable of producing

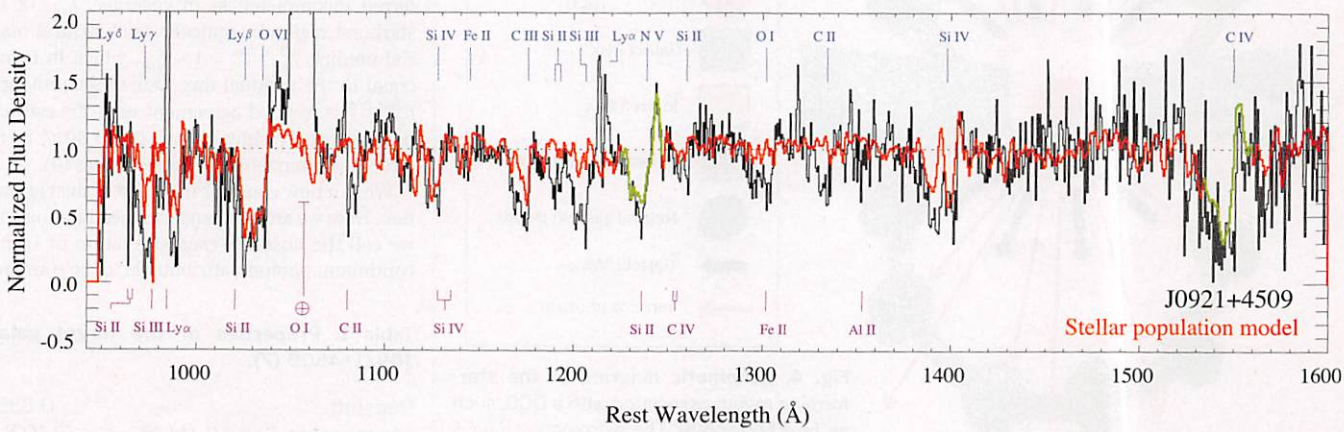

Fig. 2. Young stellar population in J0921+4509. Flux density–normalized combined spectrum from COS G140L (1040 to 1600 Å) and G130M (~950 to 1040 Å) of LBA J0921+4509 (black) overlaid with the best-fit stellar population model (Starburst99) of instantaneous star formation 3 million years ago, solar metallicity, and a Kroupa initial mass function (red). We fitted the high-ionization stellar wind transitions (shown in green) to evaluate the best stellar population model. The transitions associated with J0921+4509 are marked in blue above the spectrum; Milky Way and geocoronal features are marked in purple in the space below the spectrum. The J0921+4509 spectrum shows prominent P-Cygni profiles from the stellar winds (e.g., O VI λλ1032, 1038, N V λλ1239,1243, C IV λλ1548, 1551). This confirms the presence of a young stellar population with massive O stars in this galaxy.

substantial amounts of ionizing radiation. A stellar population model (*13*) of an instantaneous burst 3 million years ago and a Kroupa initial mass function describes our data best, thus suggesting that J0921+4509 has a large fraction of extremely young and massive stars.

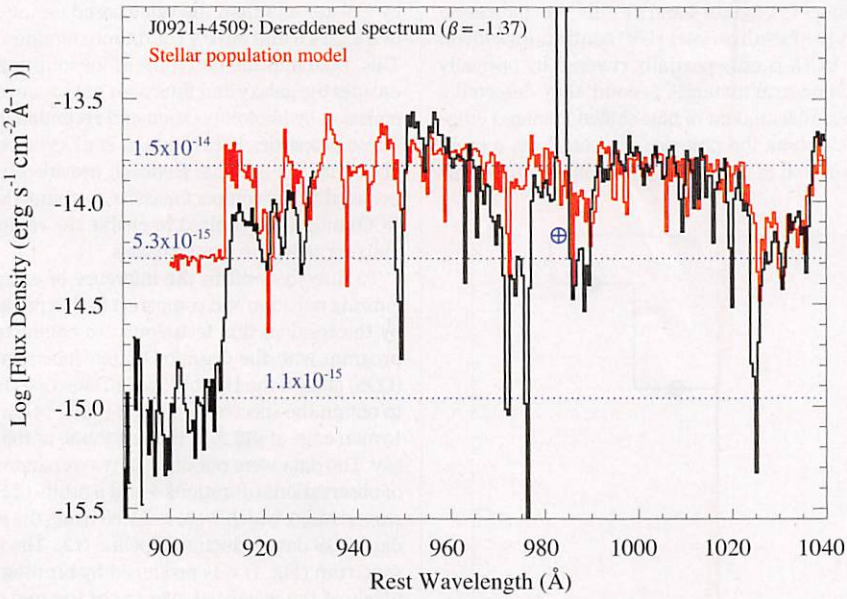

Fig. 3. Lyman continuum escape fraction. The black line denotes the COS spectrum of J0921+4509 between 890 and 1040 Å in the rest-frame of the galaxy. The spectrum was corrected for dust attenuation (*21*) corresponding to the observed UV slope of β = −1.37 in J0921+4509. The best-fit stellar population model is shown in red and has been normalized to match flux density of the data between 960 and 1040 Å. Dotted lines indicate the observed and predicted (by model) flux densities at the Lyman edge (900 to 910 Å) and at wavelengths between 1000 and 1020 Å. The ratio of strength of the observed drop to the theoretical drop represents the dust-free escape fraction.

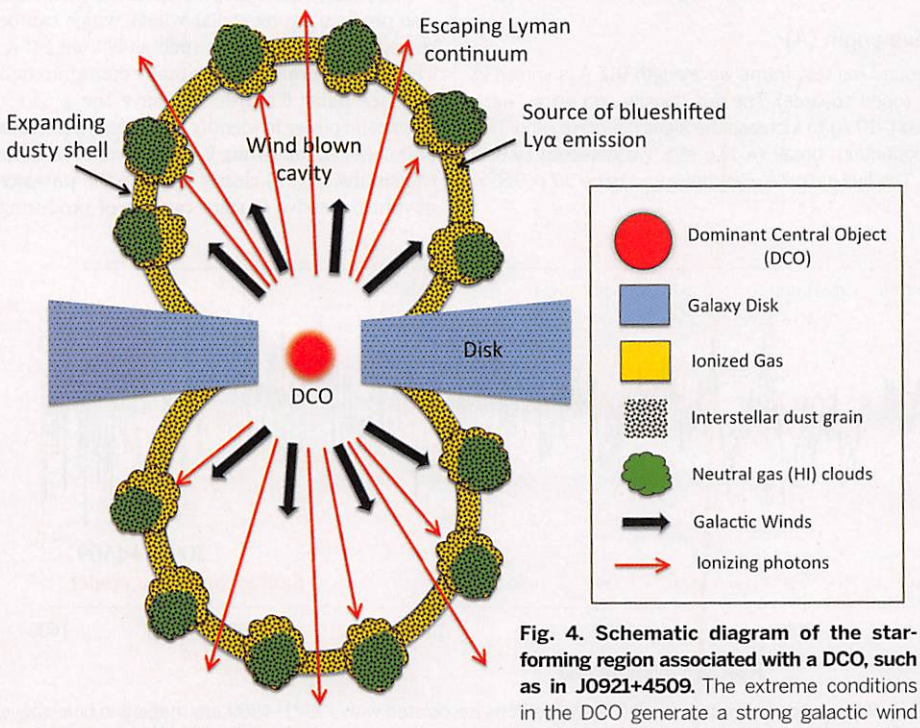

Fig. 4. Schematic diagram of the star-forming region associated with a DCO, such as in J0921+4509. The extreme conditions in the DCO generate a strong galactic wind and large quantities of ionizing flux that clear out a cavity (windblown cavity in the figure) and parts of the neutral gas cover. However, the entire region is covered by dust. The neutral gas cover contains gaps, where the gas becomes completely ionized and consequently has negligible optical depth due to photoelectric absorption of Lyman continuum photons by hydrogen. Thus, these gaps facilitate the escape of Lyman continuum and Lyman-α photons.

Before describing how we quantified the escaping ionizing radiation in this galaxy, it is important to distinguish between two sources of opacity provided by the galaxy's ISM. The first is the dust. Opacity due to dust suppresses the amount of escaping UV light by an amount that gradually and smoothly increases with decreasing wavelength. It therefore renders the UV continuum fainter and redder, but does not produce any signature across the Lyman edge at 912 Å. The second source of opacity is associated with photoelectric absorption by neutral hydrogen, which will produce a sharp drop in flux density at the Lyman edge. For simplicity, we describe these two sources of opacity separately.

First, we consider the effects of photoelectric absorption in the absence of dust (the dust-free case). The stellar population model predicts the intrinsic ratio of ionizing to nonionizing flux (i.e., the drop in flux at the Lyman edge in the absence of photoelectric absorption by the interstellar medium). A comparison of the drop in flux density between our observed data and the normalized best stellar population model describing the stellar wind lines (Fig. 3) gives us a measure of the fraction of Lyman continuum photons that suffer photoelectric absorption by atomic hydrogen in the ISM of the galaxy. In mathematical terms,

$$f_{\rm esc}^{\rm dust\ free} = \frac{\left(\frac{F_{\lambda 912-}}{F_{\lambda 912+}}\right)_{\rm observed}}{\left(\frac{F_{\lambda 912-}}{F_{\lambda 912+}}\right)_{\rm norm.\ model}} \quad (1)$$

where $F_{\lambda 912-}$ and $F_{\lambda 912+}$ are the fluxes below and above 912 Å. $F_{\lambda 912-}$ was measured by averaging the flux density over 10 Å below the Lyman break (Fig. 1). To avoid the effects of the confluence of the stellar and interstellar Lyman series absorption lines near the Lyman edge, we measured $F_{\lambda 912+}$ in a window between 1000 and 1020 Å (beyond Lyman γ). The observed drop in flux density relative to the stellar population model implies a value for $f_{\rm esc}^{\rm dust\ free} \equiv 21 \pm 5\%$. The inferred incompleteness in coverage, $f_{\rm cov}$, of the starburst region by optically thick neutral material predicts $f_{\rm esc}^{\rm dust\ free} \equiv 1 - f_{\rm cov}$, which in turn is equal to the residual flux. Our measurement of $f_{\rm esc}^{\rm dust\ free}$ is in good agreement with the estimate based on the residual flux (~20 to 30%) in the strongest interstellar absorption lines (*9*).

We can now consider the effect of dust absorption. Here we are concerned with estimating what we call the absolute escape fraction of Lyman continuum photons, attributable to the combined

Table 1. Properties of the target galaxy J0921+4509 (*7*).

Redshift	0.235
Stellar mass [log M_* ($M_\odot$)]	10.8
DCO mass [log M_* ($M_\odot$)]	9.0 to 9.2
Metallicity [12 + log(O/H)]	8.67
Star formation rate, Hα + 24 μm ($M_\odot$ year^{-1})	55.1
Dust content ($\beta_{\rm rest}$)	−1.37

effect of photoelectric absorption and dust extinction. Thus, we want to estimate the ratio between the observed luminosity of the escaping ionizing radiation and the intrinsic luminosity (in the absence of both dust and neutral hydrogen). The amount of dust absorption in the far UV is substantial in this galaxy: The ratio of UV to infrared (IR) flux is just ~10% (*7*). Assuming that the IR and UV luminosities dominate the bolometric luminosity ($L_{bol} \approx L_{UV} + L_{IR}$), we adopt the definition of the absolute escape fraction $f_{esc,abs}$ as described in (*14*):

$$f_{esc,abs} = \frac{L_{ioniz,esc}}{L_{UV} + L_{IR}} \left(\frac{L_{bol}}{L_{ioniz}} \right)_{intrinsic} \quad (2)$$

We estimate the escaping Lyman continuum luminosity $L_{ioniz,esc}$ from the data by measuring the parameter λL_λ just below the Lyman continuum break and correcting it by a factor as follows:

$$L_{ioniz,esc} = (\lambda L_\lambda)^{observed}_{\lambda=912Å} \left(\frac{L_{ioniz}}{(\lambda L_\lambda)_{\lambda=912Å}} \right)^{intrinsic} \quad (3)$$

The best-fit stellar population model predicts the intrinsic ratio L_{bol}/L_{ioniz} to be ~4, and the correction factor of Eq. 3 to be 0.9. This leads to an estimate of $f_{esc,abs} \approx 1\%$.

The difference between $f_{esc}^{dust\ free}$ and $f_{esc,abs}$ is due to the absorption of ionizing radiation by dust. It also indicates that the covering fractions of the neutral gas and the dust are not the same. Whereas the distribution of neutral gas evidently has gaps or holes, the dust almost fully covers the entire star-forming region. From this observation, we conclude that most of the dust absorption in this galaxy is associated with the ionized gas, consistent with the arguments given in (*9*). Thus, strong feedback from the starburst, in the form of ionizing radiation and shock heating by the galactic wind, is able to fully ionize holes in the distribution of neutral gas that envelops the starburst region. In these holes, the gas is fully ionized and allows the Lyman continuum photons to escape. However, the dust survives and is able to absorb both the ionizing and nonionizing UV photons (Fig. 4). The holes contain ionized gas with negligible optical depth due to photoelectric absorption for Lyman continuum photons, and also dust.

How relevant is the knowledge gained from J0921+4509 for understanding the sources responsible for reionization, given that it is highly obscured by dust? The good news is that the physics behind the creation of the holes that allow Lyman continuum to escape may be valid for any compact starburst. Such compact starburst galaxies are commonly seen at high redshifts (*15*). In fact, the highest-redshift galaxy known to date (z = 10.7) has a size (~200 pc) and stellar mass (10^8 to 10^9 $M_\odot$) (*16*) similar to the starburst in J0921+4509. On the other hand, mounting evidence from deep surveys of the early universe with the HST implies that the amount of dust absorption in star-forming galaxies is very small at the highest redshifts (*17*). This is most plausibly caused by the much lower metallicities (and hence lower dust-to-gas ratios) in these early galaxies. Recently, an intensely star-forming galaxy with very low dust and metals at $z \approx 7$ was discovered (*18*). Therefore, although dusty objects like J0921+4509 would not be good candidates for the population of galaxies that reionized the universe, similar analogs from the early universe that are compact but nearly dust-free would be excellent candidates.

It is important to reemphasize that the opacity due to neutral hydrogen in the intergalactic medium (IGM) during the epoch of reionization ($z \approx 6$ to 11) is so large that there is no hope of directly observing flux below the Lyman edge from these early galaxies and directly measuring the escape fraction. The idea that the amount of residual flux in the cores of saturated interstellar absorption lines that trace the neutral gas can serve as a proxy measurement of the escape fraction was proposed by Heckman *et al.* in 2001 (*19*), applied by Grimes *et al.* in 2009 (*14*) to a sample of local starbursts, and then applied by Heckman *et al.* (*9*) to a sample of LBAs. This idea has recently been extended to high-redshift galaxies by Jones *et al.* (*20*). Our study has validated this indirect technique. The direct value we measure for $f_{esc}^{dust\ free}$ in J0921+4509 is similar to the indirect estimate in (*9*).

REFERENCES AND NOTES

1. I. Iwata *et al.*, *Astrophys. J.* **692**, 1287–1293 (2009).
2. E. Vanzella *et al.*, *Astrophys. J.* **725**, 1011–1031 (2010).
3. D. B. Nestor, A. E. Shapley, K. A. Kornei, C. C. Steidel, B. Siana, *Astrophys. J.* **765**, 47 (2013).
4. R. E. Mostardi *et al.*, *Astrophys. J.* **779**, 65 (2013).
5. C. G. Hoopes *et al.*, *Astrophys. J. Suppl. Ser.* **173**, 441 (2007).
6. R. A. Overzier *et al.*, *Astrophys. J.* **710**, 979–991 (2010).
7. R. A. Overzier *et al.*, *Astrophys. J.* **726**, L7 (2011).
8. T. S. Gonçalves *et al.*, *Astrophys. J.* **724**, 1373–1388 (2010).
9. T. M. Heckman *et al.*, *Astrophys. J.* **730**, 5 (2011).
10. A. R. Basu-Zych *et al.*, *Astrophys. J.* **774**, 152 (2013).
11. R. A. Overzier *et al.*, *Astrophys. J.* **706**, 203–222 (2009).
12. D. Massa *et al.*, *COS Data Handbook, Version 2.0* (STScI, Baltimore, 2013).
13. C. Leitherer *et al.*, *Astrophys. J. Suppl. Ser.* **189**, 309–335 (2010).
14. J. P. Grimes *et al.*, *Astrophys. J. Suppl. Ser.* **181**, 272–320 (2009).
15. K.-H. Huang, H. C. Ferguson, S. Ravindranath, J. Su, *Astrophys. J.* **765**, 68 (2013).
16. D. Coe *et al.*, *Astrophys. J.* **762**, 32 (2013).
17. R. J. Bouwens *et al.*, http://arxiv.org/abs/1306.2950 (2013).
18. M. Ouchi *et al.*, *Astrophys. J.* **778**, 102 (2013).
19. T. M. Heckman *et al.*, *Astrophys. J.* **558**, 56–62 (2001).
20. T. A. Jones, R. S. Ellis, M. A. Schenker, D. P. Stark, *Astrophys. J.* **779**, 52 (2013).
21. I. C. Leitherer, I.-H. Li, D. Calzetti, T. M. Heckman, *Astrophys. J. Suppl. Ser.* **140**, 303–329 (2002).

ACKNOWLEDGMENTS

We thank A. Aloisi for assistance during the observations of this project, and the reviewers for their comments. S.B. is supported by a grant under program 12886 provided by NASA through a grant from the Space Telescope Science Institute, which is operated by the Association of Universities for Research in Astronomy Inc. under NASA contract NAS5-26555. Data used for this paper are publicly available in the Mikulski Archive for Space Telescopes (MAST) under programs 12886 and 11727.

1 April 2014; accepted 20 August 2014
10.1126/science.1254214

ORGANIC SYNTHESIS

Asymmetric syntheses of sceptrin and massadine and evidence for biosynthetic enantiodivergence

Zhiqiang Ma,[1]* Xiaolei Wang,[1]* Xiao Wang,[1] Rodrigo A. Rodriguez,[2] Curtis E. Moore,[3] Shuanhu Gao,[1] Xianghui Tan,[1] Yuyong Ma,[1] Arnold L. Rheingold,[3] Phil S. Baran,[2] Chuo Chen[1]†

Cycloaddition is an essential tool in chemical synthesis. Instead of using light or heat as a driving force, marine sponges promote cycloaddition with a more versatile but poorly understood mechanism in producing pyrrole–imidazole alkaloids sceptrin, massadine, and ageliferin. Through de novo synthesis of sceptrin and massadine, we show that sponges may use single-electron oxidation as a central mechanism to promote three different types of cycloaddition. Additionally, we provide surprising evidence that, in contrast to previous reports, sceptrin, massadine, and ageliferin have mismatched chirality. Therefore, massadine cannot be an oxidative rearrangement product of sceptrin or ageliferin, as is commonly believed. Taken together, our results demonstrate unconventional chemical approaches to achieving cycloaddition reactions in synthesis and uncover enantiodivergence as a new biosynthetic paradigm for natural products.

The dimeric pyrrole–imidazole alkaloids are structurally complex small molecules produced by marine sponges through reactions that are not well understood (*1*) (Fig. 1 and figs. S1 and S2). These natural products are highly polar, noncrystalline, redox labile, and pH sensitive because of their exceptionally high nitrogen content (~16% atomic composition or 15 to 30% by weight). The presence of multiple halogen atoms further contributes to their chemical instability and synthetic challenges (*2*–*21*). As depicted in Fig. 1, sceptrin (**1a**) (*22*), massadine (**2a**) (*23*, *24*), and ageliferin (**3a**) (*25*, *26*) are family members derived from formal

[2+2], [3+2], and [4+2] cycloaddition reactions of oroidin (**4a**), hymenidin (**4b**), or their congeners. Our previous studies on the de novo synthesis of ageliferins (**3**) (*4*, *14*, *15*) suggest that the biogenic dimerization of **4** is likely a radical reaction. We now describe the de novo syntheses of sceptrin (**1a**) and massadine (**2a**), using oxidative reactions that are suspected to be involved in their biosyntheses. These asymmetric syntheses along with two new crystal structures allow us to unambiguously assign the absolute stereochemistries of the pyrrole–imidazole dimers. We also demonstrate that the [3+2] dimers cannot be derived from the [4+2] or [2+2] dimers through a skeletal rearrangement reaction. Instead, a surprising enantiodivergent pathway must be involved in the biosynthesis of these alkaloids.

Sceptrin (**1a**) is the first dimeric pyrrole–imidazole alkaloid discovered in nature (*22*). Because there is insufficient light where the sponges live (20 to 30 m below the ocean surface), it is unlikely for hymenidin (**4b**) to undergo a photocycloaddition reaction to give **1a** biogenically (*2*, *22*). In addition, a [2+2] photocycloaddition reaction of **4b** would lead to the formation of racemic **1a,** whereas the isolated **1a** was optically active. Based on results of metabiosynthetic experiments, Molinski and Romo proposed an enzyme-promoted single-electron transfer (SET) mechanism for the biogenic dimerization of **4** (*27*). We believe that a SET oxidation of **4** would give radical cation $\mathbf{4}^{\bullet+}$ that is highly reactive toward [2+2] (path a) and [4+2] (path b) cycloaddition reactions to afford $\mathbf{1}^{\bullet+}$ and $\mathbf{3}^{\bullet+}$, correspondingly (Fig. 1). Subsequent back-SET would provide sceptrins (**1**) and "iso-ageliferins" (**5**) that tautomerize to ageliferins (**3**).

Massadine (**2a**) is a densely functionalized polycyclic [3+2] dimer that contains 8 contiguous stereocenters, 10 nitrogen atoms, and multiple sensitive functional groups. These structural features preclude the use of many traditional tools for its synthesis. Because enzymes that promote [3+2] cycloaddition reactions remain elusive, it is commonly believed that **2a** is derived from **5** through an oxidative skeletal rearrangement reaction (*13*, *28*, *29*). Oxidation of **5** would induce a ring-contraction reaction to give "pre-massadine" (**6**). Further oxidation of **6** would provide **2** and its congeners via different modes of cyclization (*1*, *30*). This oxidative rearrangement hypothesis was first proposed by Scheuer for palau'amine (*28*) and recently modified by us (*13*), Al-Mourabit, and Romo (*1*) to account for its revised relative stereochemistry. The chemical viability of this skeletal rearrangement through two-electron oxidation has also been demonstrated by Romo, Lovely, and us (*5*, *12*, *18*, *19*).

[1]Department of Biochemistry, The University of Texas Southwestern Medical Center, Dallas, TX 75390, USA. [2]Department of Chemistry, The Scripps Research Institute, La Jolla, CA 92037, USA. [3]Department of Chemistry and Biochemistry, University of California San Diego, La Jolla, CA 92093, USA.
*These authors contributed equally to this work †Corresponding author. E-mail: chuo.chen@utsouthwestern.edu

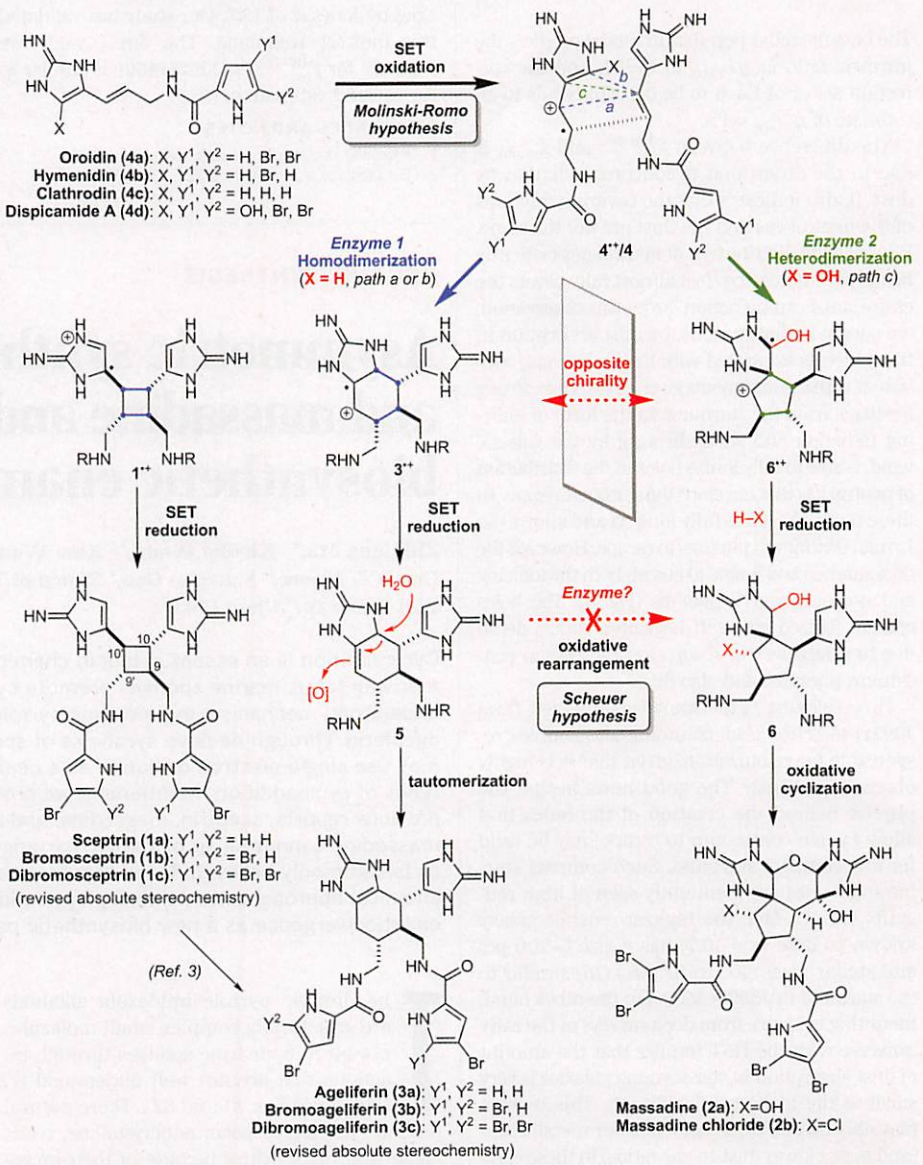

Fig. 1. The enantiodivergent biosynthetic pathways for the dimeric pyrrole-imidazole alkaloids. The biosyntheses of the [2+2] dimers sceptrins (**1**) and the [4+2] dimers ageliferins (**3**) involve a homodimerization of oroidin (**4a**) or hymenidin (**4b**). SET oxidation of **4** promotes a [2+2] cycloaddition reaction of $\mathbf{4}^{\bullet+}/\mathbf{4}$ to give $\mathbf{1}^{\bullet+}$ (path a), or a [4+2] cycloaddition reaction to give $\mathbf{3}^{\bullet+}$ (path b). Subsequent SET reduction yields **1** and **5** that aromatize to **3**. In contrast, the biosyntheses of the [3+2] dimers massadines (**2**) involve a heterodimerization of dispacamide A (**4d**) and oroidin (**4a**). SET oxidation of **4d** promotes a [3+2] cycloaddition reaction of $\mathbf{4d}^{\bullet+}/\mathbf{4a}$ to give $\mathbf{6}^{\bullet+}$. Subsequent SET reduction, protonation, and trapping with water or chloride provide "pre-massadines" (**6**). Oxidative cyclization of **6** gives massadines (**2**). The homodimerization (path a and b) and heterodimerization (path c) of **4** are enantiomeric pathways.